Design strategies for engineering soluto-inertial suspension interactions

Anirudha Banerjee, Douglas R. Vogus, and Todd M. Squires

Department of Chemical Engineering, University of California, Santa Barbara, Santa Barbara, California 93106-5080, USA



(Received 17 June 2019; published 6 November 2019)

Soluto-inertial (SI) suspension interactions allow colloidal particles to be driven large distances over sustained periods of time. These interactions involve soluto-inertial "beacons" that establish and maintain solute fluxes over long times by slowly absorbing or emitting solutes in response to changes in the surrounding solution. Suspended particles then migrate in response to solute fluxes via diffusiophoresis (DP). Beacon materials must be chosen to maintain these solute fluxes, with range and duration in mind. Here we present a general strategy to facilitate qualitative design and quantitative prediction of SI interactions for a given beacon-solute pair. Specifically, we look at two classes of SI beacons: those that partition solute and those that associate with solute. We identify the design parameters for these systems to construct a parameter space map, calculate characteristic timescales over which SI fluxes persist, and generate approximate analytical expressions for solute concentration profiles. Further, we use these expressions to predict the DP velocity of colloids interacting with beacons, noting qualitative differences between beacon sources that release solute and beacon sinks that absorb solute. Proof-of-principle experiments of beacon sources and sinks, of partitioning, and associating types highlight the basic findings. More broadly, the conceptual approach outlined here can be adapted to treat SI interactions mediated by other materials such as dissolving solids, gases, evaporating liquids, ion-exchange resins, and others.

DOI: 10.1103/PhysRevE.100.052603

I. INTRODUCTION

The ability to control and tune interactions between suspended particles, drops, and bubbles is crucial for the processing and performance of a number of everyday products such as shampoo, ink, and paint. However, the range of equilibrium colloidal interactions (e.g., electrostatic, van der Waals, depletion, and steric) is limited to less than 1 μ m in deionized, pH 7 water at room temperature, placing fundamental limits on suspension design and manipulation [1-4]. We recently introduced the concept of soluto-inertial (SI) phenomena, which can be designed to drive long-ranged and long-lived interactions in suspensions by exploiting SI "beacons" that respond slowly to changes in the local solution, emitting or absorbing solute over long times. Our experiments revealed colloidal attraction or repulsion extending millimeters in range and lasting tens of minutes [5]. More recently, we demonstrated the versatility of the SI concept with experimental demonstrations of externally triggerable SI beacons, source-sink "dipoles" formed by SI beacon pairs, and multiple SI beacons that emit distinct or reacting solutes [6].

These SI interactions have three key ingredients: (i) an SI beacon that establishes and maintains a solute flux, (ii) particles that migrate via diffusiophoresis (DP) in response to the solute flux, and (iii) solute that mediates the interaction between the beacon and particles. The term "soluto-inertia" is chosen by analogy with thermal inertia, where high-heat-capacity materials in poor heat transfer media equilibrate slowly in response to changes in external temperature while maintaining long-lasting heat flux.

Designing SI interactions for a particular application requires a solute be chosen to attract or repel colloids of interest and a beacon that slowly absorbs or releases that solute.

Here we present a systematic map of the parameter space available for SI interactions. SI beacons must have a high solute capacity (e.g., a high partition coefficient or association constant) to maintain long-lived solute gradients. Such gradients may also be established in solution by dissolving solids [7] and gases [8], by ion-exchange materials [9,10], as well as by evaporating liquids [11] to drive SI suspension interactions. Velegol *et al.* summarized a variety of distinct physical processes that establish concentration gradients and drive DP migration of colloids [12]. The strategies and guidelines laid out here should facilitate conceptual design and material selection for such systems more generally.

Moreover, geometric and material parameters must be chosen with duration and range in mind. For example, gradients in solution can be established both by source beacons that emit solute and by sink beacons that absorb solute. In both cases, the solute transport is itself described by the same equations. However, because DP velocities typically vary with $\nabla \ln C$ [13–16], or $\nabla C/C$, SI velocities remain strong even far from beacon sources (since $C \to 0$ far from the beacon) but decay more rapidly away from beacon sinks (where $C \to C_0$ away from the beacon). By contrast, liquid drops migrate in response to gradients of surface-active solute with solutocapillary velocities $V \propto \nabla C$ [17], in which case SI sources and sinks drive similar interactions. These qualitative points are discussed and experimentally demonstrated below.

Specifically, we illustrate our strategy for two distinct classes of beacons—beacons that partition solute (e.g., oils) and beacons that associate with solute (e.g., hydrogels). Our approach is as follows: First, we identify the governing equations for a specific beacon material class and isolate the design parameters. Next, we determine the timescales associated with various mass-transport processes during solute loading

and unloading. Comparing the timescales reveals the slowest rate-limiting step, which is significant conceptually and also motivates approximations that simplify the governing equations and solutions. Finally, we predict the DP velocity of colloidal particles interacting with beacon sources and sinks, and compare their qualitative features.

In our earlier work [5], we used two-dimensional (2D) cylindrical posts as beacons. However, since the mass transport in the 2D systems we modeled is inherently unsteady, our analysis here considers spheres, as will be relevant for freely suspended SI beacons.

II. SI BEACONS THAT PARTITION SOLUTE

The first class of SI beacons is those that partition solute, meaning that it is energetically favorable for solute molecules to dissolve in the beacon phase rather than in the solution phase. At equilibrium, the solute concentration C_B inside the beacon exceeds the concentration C_S in solution by the partition coefficient P [18,19], defined by

$$P = \frac{C_B}{C_S}. (1)$$

For example, an organic phase such as octanol partitions hydrophobic solutes like butanol relative to an aqueous phase [20]. Solute diffuses within each phase according to

$$\frac{\partial C_B}{\partial t} = \frac{D_B}{r^2} \frac{\partial}{\partial r} \left(r^2 \frac{\partial C_B}{\partial r} \right),\tag{2}$$

$$\frac{\partial C_S}{\partial t} = \frac{D_S}{r^2} \frac{\partial}{\partial r} \left(r^2 \frac{\partial C_S}{\partial r} \right),\tag{3}$$

where D_B and D_S are solute diffusivities in the beacon and solution phases, respectively. Imposing flux continuity at the beacon-solution interface $(r = R_B)$ gives

$$D_B \frac{\partial C_B}{\partial r} \bigg|_{R_B} = D_S \frac{\partial C_S}{\partial r} \bigg|_{R_B},\tag{4}$$

where R_B is the radius of the spherical beacon.

Additionally, we assume contact equilibrium between the solute just outside the drop ($r = R_B$ for the external solution C_S) and the solute just inside the drop (C_B), which is given simply by the partition coefficient relationship [Eq. (1)]:

$$C_B(R_B, t) = PC_S(R_B, t). \tag{5}$$

The partition coefficient [Eq. (1)] reflects a thermodynamic property related to the free-energy cost to dissolve that solute in one phase relative to the other. The contact equilibrium boundary condition [Eq. (5)] holds when molecules on either side of the boundary are energetically equivalent. This assumption may be violated when solutes are surface active, so that a surface-excess concentration Γ of adsorbed solutes takes some time to equilibrate with the concentrations on either side of the interface, or alternatively, when finite reaction kinetics limit the rate at which solutes cross that interface. The impact of reaction or adsorption kinetic limitations on otherwise diffusion-controlled systems was explored by Yariv and Frankel [21], revealing short-time dynamics where adsorptive quasiequilibrium is attained and then longer time dynamics akin to those described here. In what follows, we assume any

such interfacial dynamics to proceed very quickly and assume contact equilibrium to hold.

A beacon source unloading solute obeys the initial conditions

$$C_B(r \leqslant R_B, \ t = 0) = PC_0, \tag{6}$$

$$C_S(r > R_B, t = 0) = 0,$$
 (7)

whereas a beacon sink in solution obeys

$$C_B(r \leqslant R_B, \ t = 0) = 0,$$
 (8)

$$C_S(r > R_B, \ t = 0) = C_0.$$
 (9)

Nondimensionalizing Eqs. (2)–(4) with $C_S = C_0 \tilde{C}_S$, $C_B = PC_0 \tilde{C}_B$, $r = R_B \tilde{r}$, and $t = \tau_{SI}^0 \tilde{t}$ (where τ_{SI}^0 is as yet undefined) gives

$$\frac{R_B^2}{\tau_{\text{SI}}^0 D_B} \frac{\partial \tilde{C}_B}{\partial \tilde{t}} = \tilde{\nabla}^2 \tilde{C}_B, \tag{10}$$

$$\frac{R_B^2}{\tau_{SI}^0 D_S} \frac{\partial \tilde{C}_S}{\partial \tilde{t}} = \tilde{\nabla}^2 \tilde{C}_S,\tag{11}$$

$$\tilde{C}_B(1,\tilde{t}) = \tilde{C}_S(1,\tilde{t}),\tag{12}$$

$$P\frac{D_B}{D_S} \frac{\partial \tilde{C}_B}{\partial \tilde{r}} \bigg|_1 = \frac{\partial \tilde{C}_S}{\partial \tilde{r}} \bigg|_1. \tag{13}$$

Two nondimensional design parameters emerge: (i) the partition coefficient P and (ii) the diffusivity ratio D_r between the beacon and solution phases:

$$D_r = \frac{D_B}{D_S}. (14)$$

Three choices arise for the timescale $\tau_{\rm SI}^0$:

(i) Intrabeacon diffusion timescale τ_B , required for solute profiles to reach quasisteady state within the beacon, irrespective of what happens outside in solution:

$$\tau_B = \frac{R_B^2}{2\pi^2 D_B};$$
 (15)

(ii) Solution diffusion timescale τ_S , required for solute profiles to reach quasisteady state outside the beacon, irrespective of what happens inside:

$$\tau_S = \frac{R_B^2}{\pi^2 D_S};\tag{16}$$

(iii) Quasisteady timescale τ_{QS} , described in our earlier work [5], which arises when external mass transport is diffusion limited, yet strong partitioning ensures a slow solute release:

$$\tau_{\rm QS} = \frac{PR_B^2}{3D_{\rm S}}.\tag{17}$$

We expect the longest of the three timescales to limit the dynamics of mass transport and thus to set τ_{SI}^0 .

A. SI dynamic regimes: Partitioning beacons

For brevity, we will explicitly discuss beacon sources that release solute, noting that beacon sinks that absorb solute obey identical governing equations [Eqs. (2) and (3)] and boundary

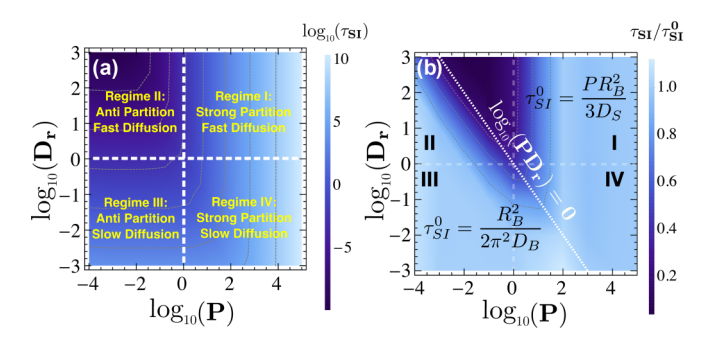


FIG. 1. SI time, τ_{SI} , required for a partitioning beacon to unload solute as a function of the partition coefficient P [Eq. (1)] and diffusivity ratio D_r [Eq. (14)]. (a) Computed SI times required for beacon to unload 63% (1-1/e) of its maximum initial concentration. Parameter space naturally divides into four qualitatively distinct solute transport regimes. (b) Scaling τ_{SI} in (a) by the combined SI timescale $\tau_{SI}^0 = \tau_{QS} + \tau_B$ [Eq. (18)] collapses all data, except in regime II, which holds no interest for SI systems.

conditions [Eqs. (5) and (4)], and hence follow similar masstransport dynamics. To quantify the extended release property of beacons, we calculate the time required for them to release 63% (1-1/e) of their initial solute content and define it as the SI time, τ_{SI} . Figure 1 shows the computed SI times and the four qualitatively distinct regimes for solute transport that naturally emerge. Most promising for sustained solute release are strongly partitioning beacons $(P \gg 1)$ for which solute diffusion may be limited externally $(D_r \gg 1, \text{ regime I})$ or internally ($D_r \ll 1$, regime IV). Antipartitioning ($P \ll 1$) may not seem promising, since solute molecules would prefer to be dissolved in the solution phase rather than the beacon phase and hence leave the beacon quickly. However, sustained solute release is actually possible if intrabeacon diffusion is slow $(D_r \ll 1, \text{regime III})$. In regime II, beacons antipartition solute $(P \ll 1)$ and intrabeacon diffusion is fast $(D_r \gg 1)$, which always leads to fast release. Thus, regime II is omitted from further consideration.

Equations (15)–(17) describe timescales associated with various solute transport processes, with the longest among them limiting the dynamics of transport. Anticipating that systems of interest for SI interactions are limited by either strong partitioning or slow intrabeacon diffusion, we construct a combined timescale τ_{SI}^0 by combining τ_{QS} [Eq. (17)] and τ_B [Eq. (15)]:

$$\tau_{\rm SI}^0 = \tau_{\rm QS} + \tau_B = \frac{PR_B^2}{3D_{\rm S}} + \frac{R_B^2}{2\pi^2 D_B}.$$
 (18)

Scaling τ_{SI} in Fig. 1(a) by this combined timescale τ_{SI}^0 then collapses all computations, except in regime II [Fig. 1(b)].

In what follows, we derive approximate transport concentration profiles in the various regimes, with results summarized in Table I.

1. Regime I - Strong partitioning, externally limited transport

Regime I corresponds to strongly partitioning beacons $(P \gg 1)$, for which internal solute diffusion is fast $(D_r \gg 1)$.

TABLE I. Design summary of beacons that partition solute.

Regime	Condition	$ au_{ m SI}^{0}$	$ ilde{C}_B$	$ ilde{C}_S$
Ι	$PD_r \gg 1$ [Eq. (19)]	$\frac{PR_B^2}{3D_S}$ [Eq. (17)]	$e^{-\tilde{t}}$ [Eq. (23)]	$\frac{\frac{e^{-\tilde{t}}}{\tilde{r}}}{[Eq. (24)]}$
III	$PD_r \ll 1$ [Eq. (25)]	$\frac{R_B^2}{2\pi^2 D_B}$ [Eq. (15)]	$\frac{2}{\pi \tilde{r}} \sin(\pi \tilde{r}) e^{-\tilde{t}/2}$ [Eq. (28)]	$2PD_r \frac{e^{-\tilde{t}/2}}{\tilde{r}}$ [Eq. (30)]
IV	$PD_r > 1$ $PD_r < 1$	$\frac{PR_B^2}{3D_S} + \frac{R_B^2}{2\pi^2 D_B}$ [Eq. (18)]	$e^{-\tilde{t}}$ $\frac{2}{\pi \tilde{r}} \sin(\pi \tilde{r}) e^{-\tilde{t}/2}$	$2PD_r \frac{e^{-\tilde{t}}}{\tilde{r}}$

Comparing the timescales from Eqs. (15)–(17) reveals the quasisteady timescale to be the slowest in this regime:

$$\frac{\tau_{\rm QS}}{\tau_B} = \frac{PR_B^2/3D_S}{R_B^2/2\pi^2D_B} \approx PD_r \gg 1,$$
 (19)

$$\frac{\tau_{\rm QS}}{\tau_S} = \frac{PR_B^2/3D_S}{R_B^2/\pi^2D_S} \approx P \gg 1,\tag{20}$$

and therefore we assume $\tau_{\rm SI}^0 \approx \tau_{\rm QS}$. Here, the beacon concentration changes so slowly that concentration profiles within and outside the beacon reach quasisteady state, and concentration gradients within the beacon can be neglected, $C_B(r,t) \sim C_B(t)$. Steady-state diffusion in spherical coordinates further implies that solute profiles outside the beacon decay like 1/r:

$$C_S(r,t) = \frac{C_B(t)}{P} \frac{R_B}{r}.$$
 (21)

Balancing the diffusion-limited outflux to the loss of solute from the beacon gives

$$\frac{4\pi R_B D_S C_B(t)}{P} = -\frac{d}{dt} \left[\frac{4}{3} \pi R_B^3 C_B(t) \right], \tag{22}$$

from which

$$C_B(t) = PC_0 e^{-\frac{3D_S}{PR_B^2}t} \Rightarrow \tilde{C}_B = \exp(-\tilde{t}), \tag{23}$$

$$C_S(r,t) = C_0 \frac{R_B}{r} e^{-\frac{3D_S}{PR_B^2}t} \Rightarrow \tilde{C}_S = \frac{\exp(-\tilde{t})}{\tilde{r}}.$$
 (24)

Computed concentration profiles (points) agree well with the analytical approximations [Eqs. (23) and (24), lines], as shown in Fig. 2.

2. Regime III - Antipartitioning, internally limited transport

Regime III involves slow solute diffusion within the beacon $(D_r \ll 1)$ and antipartitioning between the beacon and solution $(P \ll 1)$. The beacon diffusion timescale τ_B is the slowest among the three timescales [Eqs. (15)–(17)] and is expected to limit SI unloading:

$$\frac{\tau_{\rm QS}}{\tau_B} = \frac{PR_B^2/3D_S}{R_B^2/2\pi^2 D_B} \approx PD_r \ll 1,$$
 (25)

$$\frac{\tau_S}{\tau_B} = \frac{R_B^2/\pi^2 D_S}{R_B^2/2\pi^2 D_B} \approx D_r \ll 1.$$
 (26)

We therefore assume $\tau_{SI}^0 \approx \tau_B$. Since the beacon antipartitions solute, we expect $C_S \ll C_B$. Moreover, intrabeacon diffusion

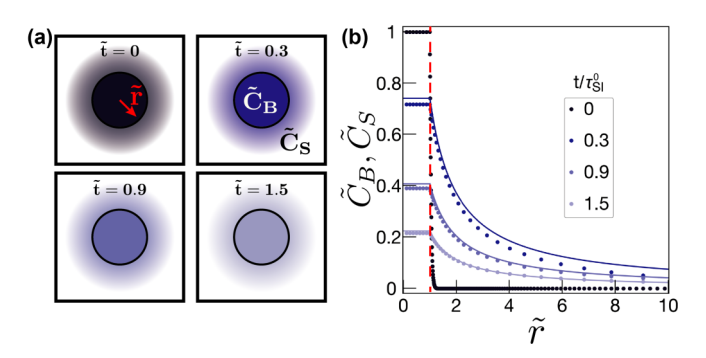


FIG. 2. Partitioning beacons, regime I: Strong partitioning and fast internal diffusion. Concentration profiles inside (\tilde{C}_B) and outside (\tilde{C}_S) the beacon vs radial distance from the center of the beacon at different times. (a) In this regime, solute concentrations inside the beacon are spatially uniform, with strong gradients outside in solution. (b) Computed profiles (points) and approximate analytical solutions [Eqs. (23) and (24), lines] show no gradients in solute concentration inside the beacon and steep gradients outside. Computations performed with P=1000 and $D_r=1000$. Time is nondimensionalized by $\tau_{\rm SI}^0 \approx \tau_{\rm QS} = PR_B^2/3D_S$ [Eq. (17)].

is slow, which implies that almost the entire concentration drop occurs within the beacon. Thus, solving Eq. (2) with an approximate boundary condition $C_B(R_B, t) = 0$ gives

$$\tilde{C}_B(\tilde{r}, \tilde{t}) = -\frac{2}{\tilde{r}} \sum_{n=1}^{\infty} \frac{(-1)^n}{n\pi} \sin(n\pi \tilde{r}) \exp\left(-\frac{n^2 \tilde{t}}{2}\right), \quad (27)$$

which can be simplified at long times $(t > \tau_{SI}^0)$ by simply retaining the slowest decaying eigenmode (n = 1) to yield

$$\tilde{C}_B(\tilde{r}, \tilde{t}) \approx \frac{2}{\pi \tilde{r}} \sin \pi \tilde{r} \exp\left(-\frac{\tilde{t}}{2}\right).$$
 (28)

Although the solution concentration C_S is small, DP migration is driven by solute gradients in solution. Therefore, to predict the DP velocity of particles generated by beacons in this regime, we must determine an approximate expression for C_S . The concentration profile outside the beacon evolves quasisteadily as 1/r, since internal mass transport is slow. The flux balance condition [Eq. (4)] then gives

$$\tilde{C}_{S}(\tilde{r}, \tilde{t}) = -\frac{PD_{r}}{\tilde{r}} \left. \frac{\partial \tilde{C}_{B}}{\partial \tilde{r}} \right|_{\tilde{r}=1}.$$
(29)

From Eqs. (28) and (29), we obtain

$$\tilde{C}_{S}(\tilde{r}, \tilde{t}) \approx 2PD_{r} \frac{\exp(-\tilde{t}/2)}{\tilde{r}}.$$
 (30)

Since P and D_r are both small in this regime, $\tilde{C}_S \propto PD_r$ is even smaller. Figure 3 shows good agreement between the approximate analytical solution [Eqs. (27) and (30), lines] and the full computed solution [points].

The DP migration velocity of particles are predicted [13,22] to obey

$$u_{\rm DP} = D_{\rm DP} \nabla \ln C_{\rm S}, \tag{31}$$

where D_{DP} is the DP mobility of the particles. Equation (31) implies that even when ∇C_S is small, the DP velocity can be appreciable if C_S is also small. Therefore, observable DP

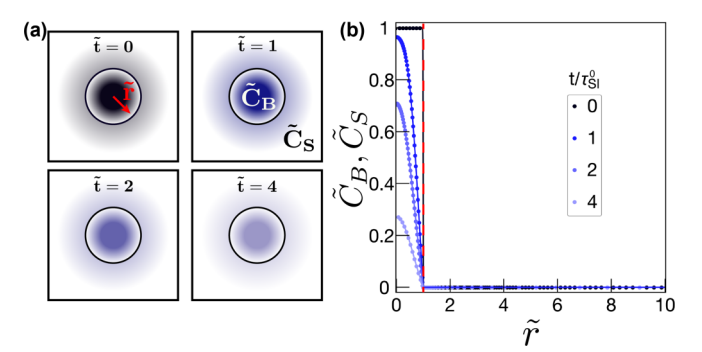


FIG. 3. Partitioning beacons, regime III: Antipartitioning and slow internal diffusion. Concentration profiles inside (\tilde{C}_B) and outside (\tilde{C}_S) the beacon vs radial distance from the center of the beacon at different times. (a) In this regime, solute concentration drops significantly within the beacon itself, with relatively weak gradients in solution. (b) Computations (points) and approximate analytical solutions [Eqs. (27) and (30), lines] show the large concentration gradients within the beacon and the weak gradients outside. Computations performed with P = 0.001 and $D_r = 0.001$. Time is nondimensionalized by $\tau_{SI}^0 \approx \tau_B = R_B^2/2\pi^2 D_B$ [Eq. (15)].

colloidal migration may still be driven by SI beacons in this regime.

3. Regime IV - Strong partitioning, slow intrabeacon diffusion

In regime IV, solute partitioning in the beacon is strong like in regime I; however, internal diffusion is slow like in regime III. Mass-transport limitations depend upon which process is the slowest. A flux balance across the beacon-solution interface reveals the timescale for SI unloading in this regime.

Under the quasi-steady-state approximation, the solute concentration profile outside the beacon can be expressed as

$$C_S = \frac{C_B^i}{R} \frac{R_B}{r},\tag{32}$$

where C_B^i is solute concentration at the beacon interface. The diffusive solute flux leaving the beacon,

$$J_S = D_S \frac{C_B^i}{PR_B},\tag{33}$$

is balanced by a flux within the beacon,

$$J_B \approx D_B \frac{C_B^0 - C_B^i}{R_B},\tag{34}$$

where C_B^0 is the concentration at the center of the beacon. Equating these two fluxes yields

$$C_B^i \approx C_B^0 \left(\frac{PD_r}{1 + PD_r}\right).$$
 (35)

Balancing the loss of solute to the diffusion-limited outflux from the beacon [Eq. (33)] gives

$$\frac{4}{3}\pi R_B^3 \frac{dC_B^0}{dt} \approx -4\pi R_B^2 \frac{D_S C_B^i}{P R_B}.$$
 (36)

Approximating $C_B^0 \propto e^{-t/\tau_{\rm SI}^0}$ leads to

$$\frac{R_B^2 C_B^0}{3\tau_{\rm SI}^0} = \frac{D_S C_B^i}{P},\tag{37}$$

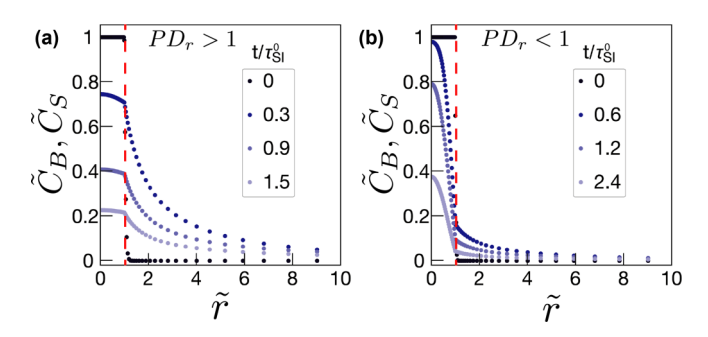


FIG. 4. Partitioning beacons, regime IV: Strong partitioning and slow internal diffusion. Concentration profiles inside (\tilde{C}_B) and outside (\tilde{C}_S) the beacon vs radial distance from the center of the beacon at different time steps. (a) When $PD_r > 1$, concentration profiles resemble those of regime I (Fig. 2), where diffusion is externally limited. (b) However, when $PD_r < 1$, internal transport is limiting and profiles look like those of regime III (Fig. 3). Time is scaled by $\tau_{\rm SI}^0 = \tau_{\rm QS} + \tau_B$. Computations in (a) performed with P = 1000 and $D_r = 0.01$, whereas computations in (b) performed with P = 100 and $D_r = 0.001$. Time is nondimensionalized by $\tau_{\rm SI}^0 = PR_B^2/3D_S + R_B^2/2\pi^2D_B$ [Eq. (18)].

which ultimately results in

$$\tau_{\rm SI}^0 \approx \frac{PR_B^2}{3D_S} \left(1 + \frac{1}{PD_r} \right) = \tau_{\rm QS} + \tau_B 2\pi^2.$$
(38)

Two extremes of τ_{SI}^0 then emerge from Eq. (38). Internal solute diffusion is rate limiting when $PD_r \ll 1$, in which case

$$\tau_{\rm SI}^0 \approx \frac{PR_B^2}{3D_{\rm S}} \frac{1}{PD_{\rm r}} \approx \frac{R_B^2}{D_B} \approx \tau_B,\tag{39}$$

as in regime III. Very strong partitioning $(PD_r \gg 1)$, on the other hand, gives the quasisteady timescale as in regime I,

$$\tau_{\rm SI}^0 \approx \frac{PR_B^2}{3D_{\rm S}} = \tau_{\rm QS}.\tag{40}$$

Intermediate examples (i.e., regions with $PD_r < 1$ or $PD_r > 1$) are shown in Fig. 4.

B. Particle velocity near beacon sources and sinks

Solute gradients can be generated in solution by both beacon sources that release solute and beacon sinks that absorb solute. Because sources and sinks are governed by the same mass-transport equations, τ_{SI}^0 does not discriminate between solute loading or unloading. The resulting DP velocities in suspension, however, differ dramatically for these two situations, because DP velocities do not vary linearly in ∇C_S but instead scale with $\nabla \ln C_S$.

Regime I beacons that strongly partitioned solute highlight these differences. The concentration outside a beacon source evolves according to [Eq. (24)]

$$\tilde{C}_{S}^{\text{source}} = \frac{\exp(-\tilde{t})}{\tilde{r}},$$
 (41)

yet beacon sinks establish

$$\tilde{C}_{\mathcal{S}}^{\text{sink}} = 1 - \frac{1}{\tilde{r}} \exp(-\tilde{t}). \tag{42}$$

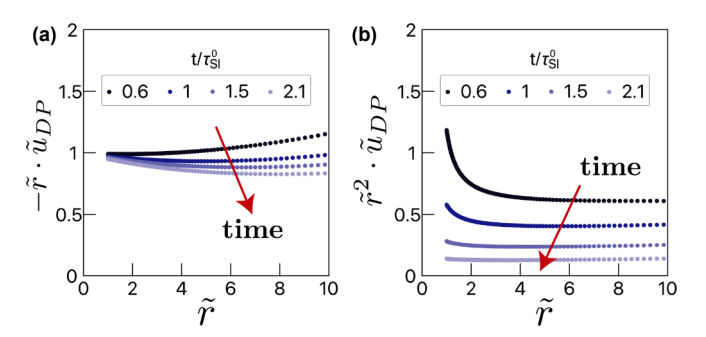


FIG. 5. Diffusiophoretic velocity of particles driven by beacon (a) sources vs (b) sinks in regime I. (a) The SI migration driven by sources decays like \tilde{r}^{-1} [Eq. (43)]. By contrast, velocities generated by SI sinks decay more rapidly in space (\tilde{r}^{-2}) and exponentially in time [Eq. (45)].

The particle DP velocities driven by regime I beacon sources and sinks can then be evaluated using Eq. (31). SI sources drive DP velocities

$$\tilde{u}_{\mathrm{DP}}^{\mathrm{source}}(\tilde{r}) = -\frac{1}{z},$$
 (43)

whereas beacon sinks drive

$$\tilde{u}_{\mathrm{DP}}^{\mathrm{sink}}(\tilde{r}, \tilde{t}) = \frac{1}{\tilde{r}^2} \frac{\exp(-\tilde{t})}{1 - \frac{1}{\tilde{z}} \exp(-\tilde{t})}.$$
(44)

In both cases, $u_{\rm DP}$ is nondimensionalized by $D_{\rm DP}/R_B$.

One can immediately draw a striking contrast between the $u_{\rm DP}$ expressions for sources [Eq. (43)] and sinks [Eq. (44)]. At large times ($t > \tau_{\rm SI}^0$), SI migration around SI sinks decays exponentially [Fig. 5(b)] via

$$\tilde{u}_{\mathrm{DP}}^{\mathrm{sink}}(\tilde{r}, \tilde{t} > 1) = \frac{\exp(-\tilde{t})}{\tilde{r}^2},\tag{45}$$

whereas SI interactions around SI source beacons show no apparent temporal dependence [Fig. 5(a), Eq. (43)]. Moreover, DP velocities for SI beacon sinks decay more quickly in space $[\tilde{r}^{-2}, \text{Fig. 5(b)}]$ than beacon sources $[\tilde{r}^{-1}, \text{Fig. 5(a)}]$.

In regime III, where mass transport is limited internally, $u_{\rm DP}$ decays even faster for beacon sinks because most of the solute concentration drops across the beacon. Thus, gradients in solution are weak while background concentrations are high. Since $u_{\rm DP}$ scales as $\nabla C_S/C_S$, DP velocities for such sinks become vanishingly small. On the other hand, strong velocities can still be obtained with beacon sources in this regime, since small gradients are accompanied by small concentrations in solution, and ratios of ∇C_S to C_S remain appreciable. A greater flexibility in material selection can hence be achieved with beacon sources (either regimes I, III or IV), whereas materials for effective beacon sinks require rapid internal mass transport that is only realized in regime I.

III. SI BEACONS THAT ASSOCIATE WITH SOLUTE

The second class of beacons involves materials with high surface-to-volume ratio that associate with particular solutes and therefore can store solute via adsorption. These materials include polymer hydrogels [23], mesoporous silica particles [24], and supraparticles [25]. The solute molecules

associate with the beacon material with association constant K; the greater the value of K, the higher the beacon's solute capacity.

Here we model the mass transport within these porous beacon materials assuming linear adsorption-desorption kinetics, $C_{\text{free}} <=> [k_1][k_{-1}]C_{\text{ads}}$, where C_{free} and C_{ads} are the concentrations of the free (unbound) and adsorbed species, respectively. k_1 and k_{-1} are the rates of adsorption and desorption, respectively, and the association constant is defined as

$$K = \frac{k_1}{k_{-1}}. (46)$$

The concentration of free and adsorbed solute species within the beacon evolves according to

$$\frac{dC_{\text{ads}}}{dt} = k_1 C_{\text{free}} - k_{-1} C_{\text{ads}},\tag{47}$$

$$\frac{\partial C_{\text{free}}}{\partial t} = \frac{D_{\text{free}}}{r^2} \frac{\partial}{\partial r} \left(r^2 \frac{\partial C_{\text{free}}}{\partial r} \right) + k_{-1} C_{\text{ads}} - k_1 C_{\text{free}}. \tag{48}$$

The adsorbed molecules are bound to the beacon material and hence do not diffuse, while the free solute molecules diffuse with a diffusivity D_{free} . The solute transport in solution obeys Eq. (3). Diffusion of solute within these porous materials is usually slower than the diffusion in bulk solution due to the tortuous diffusion path [26,27]. To that end, and to reduce the complexity of the design space, the ratio of free solute diffusivity in the beacon and in solution is assumed to be small,

$$D_r = \frac{D_{\text{free}}}{D_S} \ll 1. \tag{49}$$

The boundary conditions at the beacon-solution interface $(r = R_B)$ are

$$C_{\text{free}}(R_R, t) = C_S(R_R, t), \tag{50}$$

$$D_{\text{free}} \frac{\partial C_{\text{free}}}{\partial r} \bigg|_{R_B} = D_S \frac{\partial C_S}{\partial r} \bigg|_{R_B}.$$
 (51)

For a beacon source unloading solute, the following initial conditions hold:

$$C_{\text{free}}(r \leqslant R_B, \ t = 0) = C_0,$$
 (52)

$$C_{\text{ads}}(r \leqslant R_B, \ t = 0) = KC_0,$$
 (53)

while for a beacon sink loading solute, the initial conditions are

$$C_{\text{free}}(r \leqslant R_B, \ t = 0) = 0, \tag{54}$$

$$C_{\text{ads}}(r \leqslant R_B, \ t = 0) = 0.$$
 (55)

The initial condition for solute concentration in solution is given by Eqs. (7) and (9) for solute unloading (source) and loading (sink), respectively. Nondimensionalizing Eqs. (47)–(51) with $C_{\text{free}} = C_0 \tilde{C}_{\text{free}}$, $C_{\text{ads}} = K C_0 \tilde{C}_{\text{ads}}$, $C_S = C_0 \tilde{C}_S$, $r = R_B \tilde{r}$, and $t = \tau_{\text{SI}}^0 \tilde{t}$ gives

$$\frac{K}{\tau_{\rm SI}^0 k_1} \frac{\partial \tilde{C}_{\rm ads}}{\partial \tilde{t}} = \tilde{C}_{\rm free} - \tilde{C}_{\rm ads},\tag{56}$$

$$\frac{R_B^2}{\tau_{\text{SI}}^0 D_{\text{free}}} \frac{\partial \tilde{C}_{\text{free}}}{\partial \tilde{t}} = \tilde{\nabla}^2 \tilde{C}_{\text{free}} + \frac{k_1 R_B^2}{D_{\text{free}}} (\tilde{C}_{\text{ads}} - \tilde{C}_{\text{free}}), \tag{57}$$

$$\tilde{C}_{\text{free}}(1,\tilde{t}) = \tilde{C}_{S}(1,\tilde{t}),\tag{58}$$

$$\frac{D_{\text{free}}}{D_S} \frac{\partial \tilde{C}_{\text{free}}}{\partial \tilde{r}} \bigg|_{1} = \left. \frac{\partial \tilde{C}_S}{\partial \tilde{r}} \right|_{1}.$$
 (59)

Two nondimensional design parameters emerge: (i) the association constant K, and (ii) the Damköhler number,

$$Da = \frac{k_1 R_B^2}{D_{\text{free}}},\tag{60}$$

which expresses the relative rates of solute adsorption k_1 and diffusion D_{free}/R_R^2 .

Three timescales (τ_{SI}^0) are relevant in these systems:

(i) An effective diffusion timescale τ_B^{eff} , required for solute profiles inside the beacon to reach steady state when adsorption-desorption equilibration is rapid, such that $C_{\text{ads}} = KC_{\text{free}}$. Adding Eqs. (47) and (48), and using this equilibrium condition reveals

$$\frac{\partial C_{\text{free}}}{\partial t} = \frac{D_{\text{free}}}{1 + K} \frac{1}{r^2} \frac{\partial}{\partial r} \left(r^2 \frac{\partial C_{\text{free}}}{\partial r} \right), \tag{61}$$

which implies that solute diffuses within the beacon with an effective diffusion coefficient [28]:

$$D_{\text{eff}} = \frac{D_{\text{free}}}{1 + K}.\tag{62}$$

The effective diffusion timescale $\tau_B^{\rm eff}$ is therefore given by:

$$\tau_B^{\text{eff}} = \frac{R_B^2}{2\pi^2 D_{\text{eff}}} = \frac{R_B^2 (1+K)}{2\pi^2 D_{\text{free}}} = (1+K)\tau_B.$$
(63)

(ii) The adsorption timescale τ_{ads} , required for free solute molecules to adsorb onto the beacon:

$$\tau_{\rm ads} = \frac{1}{k_1};\tag{64}$$

(iii) The desorption time τ_{des} , required for the adsorbed solute species to desorb from the beacon:

$$\tau_{\rm des} = \frac{1}{k_{-1}}.\tag{65}$$

Since solute diffusion in the bulk is considered to be fast compared to diffusion and desorption of solute within the beacon, we do not include the solution diffusion timescale, $\tau_S = R_B^2/\pi^2 D_S$, in our analysis. We expect the longest of the three timescales [Eqs. (63)–(65)] to limit the dynamics of solute transport and therefore to set $\tau_{\rm SI}^0$.

A. SI dynamic regimes: Associating beacons

We calculate the SI unloading time τ_{SI} for an associating beacon source that unloads solute as a function of the association constant K [Eq. (46)] and the Damköhler number Da [Eq. (60)]. Four distinct regimes for mass transport naturally emerge, with qualitatively distinct transport properties as shown in Fig. 6(a). Most promising for sustained solute release are beacons that strongly associate with solute ($K \gg 1$), for which solute diffusion may be slow (regime I, Da $\gg 1$) or fast (regime IV, Da $\ll 1$). Although weakly associating

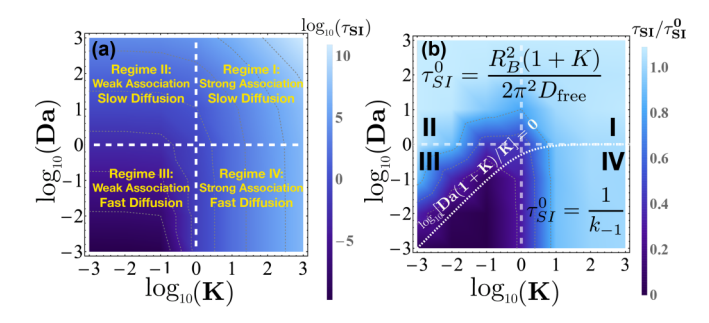


FIG. 6. SI time, τ_{SI} , required for an associating beacon to unload solute as a function of the association constant, K [Eq. (46)] and the Damköhler number Da [Eq. (60)]. (a) Computed SI times required for beacon to unload 63% (1-1/e) of its maximum initial concentration. Parameter space naturally divides into four qualitatively distinct solute transport regimes. (b) Scaling τ_{SI} in (a) by the combined SI timescale $\tau_{SI}^0 = \tau_{des} + \tau_B^{eff}$ [Eq. (66)] collapses all data except in regime III, which holds no interest for SI systems.

beacons may not seem promising for sustained solute fluxes, long τ_{SI} may also be achieved when intrabeacon diffusion is slow (regime II, Da \gg 1). Regime III corresponds to weakly associating beacons ($K \ll 1$), for which solute diffusion is fast, giving beacons with low solute capacity. We therefore omit them from further consideration.

In each of these regimes, the longest of the three timescales $\tau_B^{\rm eff}$ [Eq. (63)], $\tau_{\rm ads}$ [Eq. (64)], and $\tau_{\rm des}$ [Eq. (65)] should govern the rate of solute transport. However, since SI unloading in the regimes considered here is either limited by internal diffusion or solute desorption from the beacon, and never by solute adsorption, we combine Eqs. (63) and (65) to obtain a general expression for the longest SI unloading timescale:

$$\tau_{\rm SI}^0 = \tau_{\rm des} + \tau_B^{\rm eff} = \frac{1}{k_{-1}} + \frac{R_B^2(1+K)}{2\pi^2 D_{\rm free}}.$$
 (66)

Scaling τ_{SI} in Fig. 6(a) by this combined timescale collapses all data, except in regime III, as shown in Fig. 6(b).

In what follows, we derive approximate solute concentration profiles in the various regimes, with results summarized in Table II.

1. Regimes I and II: Intrabeacon solute diffusion slower than adsorption-desorption kinetics

Regimes I and II correspond to slow intrabeacon diffusion relative to adsorption-desorption. The Damköhler number is large in these systems (Da \gg 1), and the effective diffusion

timescale [Eq. (63)] is much greater than the adsorption [Eq. (64)] and desorption [Eq. (65)] timescales,

$$\frac{\tau_B^{\text{eff}}}{\tau_{\text{des}}} = \frac{R_B^2 (1+K)/2\pi^2 D_{\text{free}}}{1/k_{-1}} \approx \frac{\text{Da}(1+K)}{K} \gg 1,$$
 (67)

$$\frac{\tau_B^{\text{eff}}}{\tau_{\text{ads}}} = \frac{R_B^2 (1+K)/2\pi^2 D_{\text{free}}}{1/k_1} \approx \text{Da}(1+K) \gg 1.$$
 (68)

We therefore expect $\tau_B^{\rm eff}$ to limit the dynamics of SI unloading and assume $\tau_{\rm SI}^0 \approx \tau_B^{\rm eff}$. Since mass transport is diffusion limited, adsorption-desorption is in quasiequilibrium in these regimes, i.e., $\tilde{C}_{\rm ads} = \tilde{C}_{\rm free}$. Moreover, the rate-limiting process of intrabeacon diffusion suggests that almost all concentration drops within the beacon. We therefore impose $C_{\rm free}$, $C_{\rm ads} \approx 0$ at the beacon boundary $(r=R_B)$, in which case $\tilde{C}_{\rm free}$ and $\tilde{C}_{\rm ads}$ are given by

$$\tilde{C}_{\text{free}} = \tilde{C}_{\text{ads}} = \tilde{C}_{\text{total}}(\tilde{r}, \tilde{t})
= -\frac{2}{\tilde{r}} \sum_{n=1}^{\infty} \left(\frac{(-1)^n}{n\pi} \right) \sin(n\pi\tilde{r}) \exp\left(-\frac{n^2\tilde{t}}{2} \right).$$
(69)

 C_{total} is the total beacon solute concentration, $C_{\text{total}} = C_{\text{free}} + C_{\text{ads}}$, which is normalized by $C_0 + KC_0$ to give

$$\tilde{C}_{\text{total}} = \frac{C_{\text{total}}}{C_0 + KC_0}.$$
(70)

Equation (69) can be further simplified at long times by keeping the slowest decaying eigenmode (n = 1) to obtain

$$\tilde{C}_{\text{free}} = \tilde{C}_{\text{ads}} = \tilde{C}_{\text{total}}(\tilde{r}, \tilde{t}) \approx \frac{2}{\pi \tilde{r}} \sin \pi \tilde{r} \exp\left(-\frac{\tilde{t}}{2}\right).$$
 (71)

Although solute concentration in solution C_S is small, because most of the concentration drops within the beacon, an approximate expression for C_S is required to predict DP velocity of particles. We therefore estimate C_S by assuming quasisteady decay and balancing the diffusive solute flux across the beacon interface $(r = R_B)$ according to Eq. (51) to obtain

$$\tilde{C}_{S}(\tilde{r}, \tilde{t}) \approx 2D_{r} \frac{\exp(-\tilde{t}/2)}{\tilde{r}}.$$
 (72)

Figure 7 compares the full computed concentration profiles (points) with the approximate analytical solutions [Eqs. (69) and (72), lines].

2. Regime IV: Strong association, desorption-limited transport

Regime IV involves strongly associating beacons ($K \gg 1$), for which intrabeacon diffusion is fast relative to adsorption-

TABLE II. Design summary of SI beacons that associate with solutes.

Regime	Condition	$ au_{ m SI}^{0}$	$ ilde{C}_{ ext{free}}$	$ ilde{C}_{ m ads}$	$ ilde{C}_{ ext{total}}$	$ ilde{C}_S$
I & II	$\frac{\frac{\text{Da}(1+K)}{K} \gg 1}{\text{[Eq. (67)]}}$	$\frac{R_B^2(1+K)}{2\pi^2 D_{\text{free}}}$ [Eq. (63)]	$\frac{\frac{2}{\pi \tilde{r}}\sin(\pi \tilde{r})e^{-\tilde{t}/2}}{\text{[Eq. (71)]}}$	$ ilde{C}_{ ext{free}}$	$ ilde{C}_{ ext{free}}$	$2D_r \frac{e^{-\tilde{t}/2}}{\tilde{r}}$ [Eq. (72)]
IV	$\frac{\frac{\text{Da}(1+K)}{K} \ll 1}{\text{[Eq. (73)]}}$	$\frac{\frac{1}{k_{-1}}}{[Eq. (65)]}$	pprox 0	$e^{-\tilde{t}}$ [Eq. (75)]	$ ilde{C}_{ m ads}$	$\frac{\underline{D_r}\underline{Da}}{3}\frac{e^{-\tilde{t}}}{\tilde{r}}$ [Eq. (77)]

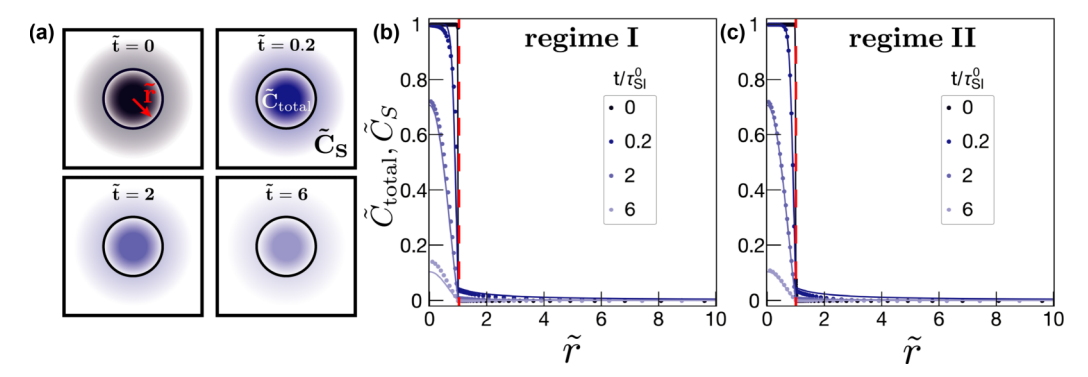


FIG. 7. Associating beacons, regimes I and II: Internal solute diffusion is slower than adsorption-desorption kinetics. Concentration profiles inside (\tilde{C}_{total}) and outside (\tilde{C}_{S}) the beacon vs radial distance from the center of the beacon at different time steps. (a) In these regimes, solute concentration drops significantly within the beacon itself, with relatively weak gradients in solution. (b), (c) Concentration profiles computed numerically (points) and analytical approximations [Eqs. (69) and (72), lines] show the strong gradients within the beacon and weak gradients outside in regimes I and II, respectively. Computations in (b) performed with K = 100, Da = 100, and $D_r = 0.01$, while computations in (c) performed with K = 0.01, Da = 1000, and $D_r = 0.01$. Time is nondimensionalized by $\tau_{SI}^0 \approx \tau_R^{eff} = R_R^2(1 + K)/2\pi^2 D_{free}$ [Eq. (63)].

desorption (Da \ll 1). In this regime, the solute desorption timescale is rate limiting:

$$\frac{\tau_B^{\text{eff}}}{\tau_{\text{des}}} = \frac{R_B^2 (1+K)/2\pi^2 D_{\text{free}}}{1/k_{-1}} \approx \frac{\text{Da}(1+K)}{K} \ll 1, \quad (73)$$

$$\frac{\tau_{\text{ads}}}{\tau_{\text{des}}} = \frac{1/k_1}{1/k_{-1}} = \frac{1}{K} \ll 1,$$
(74)

and therefore we assume $\tau_{\rm SI}^0 \approx \tau_{\rm des}$. Rapid solute diffusion renders concentration profiles inside the beacon to be spatially uniform, $C_{\rm total}(r,t) \sim C_{\rm total}(t)$. In fact, $C_{\rm free} \sim 0$ in this regime, since any solute molecule that desorbs from the beacon material quickly diffuses away. Equation (47) then gives

$$\tilde{C}_{\text{ads}}(\tilde{t}) = \tilde{C}_{\text{total}}(\tilde{t}) = \exp(-\tilde{t}).$$
 (75)

Since solute transport is limited by internal desorption, solution concentration profiles C_S outside the beacon evolve quasisteadily. Balancing the diffusive outflux to the loss of solute from the beacon gives

$$4\pi R_B^2 D_S \frac{\partial C_S}{\partial r} \bigg|_{R_D} = \frac{\partial}{\partial t} \int_0^{R_B} 4\pi r^2 C_{\text{total}}(r, t) dr, \tag{76}$$

from which

$$\tilde{C}_S = \frac{D_r \text{Da}}{3} \frac{\exp(-\tilde{t})}{\tilde{r}}.$$
(77)

Figure 8 compares the approximate analytical solutions [Eqs. (75) and (77), lines] with numerical computations (points).

IV. EXPERIMENTAL REALIZATIONS

Any SI application requires beacons to sustain solute fluxes. In the discussions above, we examined two classes of beacon materials that achieve such sustained release, either through solute partitioning or association. While theoretical analysis and numerical computations enabled prediction of the range and duration of SI migration, we now turn to experimental realizations of these systems.

Our previous demonstration of the SI effect used SI beacon sources made out of polyethylene-glycol diacrylate (PEG-DA) to sustain sodium dodecyl sulfate (SDS) gradients and drive SI particle migration over tens of minutes (Fig. 9) [5]. Although we couched the hydrogel as a partitioning beacon, it is more appropriate to use the adsorption-desorption model presented here in Sec. III. In fact, PEG-DA hydrogels are known to strongly associate with SDS ($K \gg 1$) [29] as well as retard internal diffusion of SDS molecules (Da $\gg 1$), thereby placing this system in regime I of the parameter map shown in Fig. 6. The solution concentration profile C_S [Eq. (72)] exhibits the same 1/r quasisteady decay in position and exponential decay in time as for partitioning beacons [Eq. (24)]. We therefore expect SI velocities driven by associating and partitioning beacon sources in regime I to behave in a similar manner [Eq. (43)].

Note, however, that Eq. (43) is valid only for DP velocities generated by three-dimensional (3D), spherical beacon sources. By contrast, the experiment shown in Fig. 9(a) is 2D in nature, with DP migration driven by a cylindrical

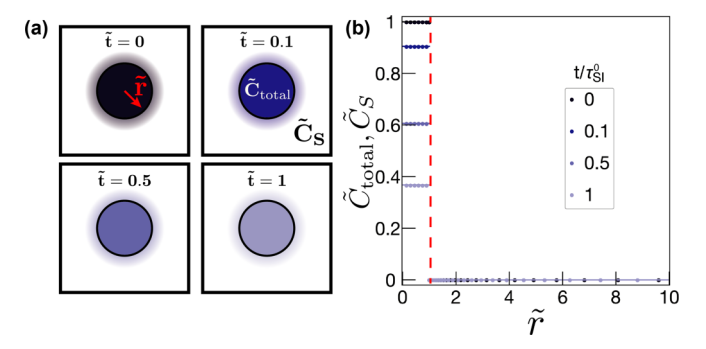


FIG. 8. Associating beacons, regime IV: Fast internal diffusion, mass transport is solute desorption limited. Concentration profiles inside (\tilde{C}_{total}) and outside (\tilde{C}_{S}) the beacon vs radial distance from the center of the beacon at different times. (a) In regime IV, solute concentration profiles are spatially uniform within the beacon, while concentrations outside in solution are small. (b) Profiles calculated numerically (points) and analytical approximations [Eqs. (75) and (77), lines] show the spatially uniform nature of the concentrations inside and small concentrations outside the beacon. Computations performed with K=1000, Da = 0.01, and $D_r=0.01$. Time is nondimensionalized by $\tau_{SI}^0 \approx \tau_{des} = 1/k_{-1}$ [Eq. (65)].

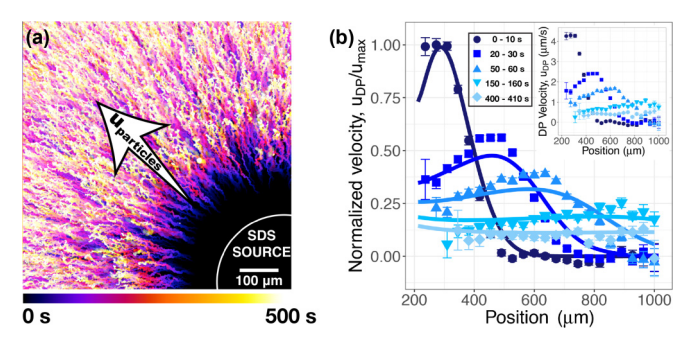


FIG. 9. DP migration of colloids driven by an SI source. (a) A PEG-DA beacon source that strongly associates with SDS, establishes an SDS gradient, and induces DP migration of neighboring colloids. Negatively charged polystyrene particles move down the SDS gradient, away from the source. (b) Comparing the experimentally measured velocities to the DP migration velocity computed using Eq. (31) in polar coordinates shows good agreement. Since the DP mobility of colloids is not known *a priori*, measured and computed velocities are normalized by the maximum measured and computed values, respectively, to enable direct comparison. Inset shows the raw experimentally tracked particle velocities. Data for (b) is adapted from [5].

beacon post. We therefore do not expect DP velocities in this case to be independent of time and evolve as 1/r according to Eq. (43). Nevertheless, velocities can be predicted using $u_{\rm DP} \propto \nabla \ln C_S$ [Eq. (31)] in polar coordinates, predictions from which agree well with previously published measurements [5], adapted in Fig. 9(b).

Figure 10 shows an SI beacon that *partitions* solute instead of *associating* with the solute. Here, octanol serves as the beacon phase and partitions butanol, with an octanol-water partition coefficient $P_{\rm ow} \approx 8$ [20]. The beacon therefore establishes long-lasting butanol gradients, driving long-range migration of decane drops over tens of minutes.

Rather than DP, decane drops migrate in butanol gradients via soluto-capillary migration [17]. Butanol reduces the surface tension of the suspended oil drops in water. Therefore, the side of the oil drop directly facing the butanol source has a lower surface tension than the side facing away from the source. The surface tension gradient along the droplet surface drives a Marangoni flow towards the high-surface-tension side, which in turn propels the drop to move in the opposite direction. Oil drops thus migrate up butanol gradients, i.e., towards beacon sources [Fig. 10(a)], or away from beacon sinks [Fig. 10(c)].

Soluto-capillary migration velocities (u_{SC}) scale with ∇C_S [17] instead of the $\nabla \ln C_S$ in DP. We therefore use $u_{SC} = D_{SC} \nabla C_S$ to model the velocities observed in Figs. 10(a) and 10(c). Assuming D_{SC} to be a constant that does not depend on C_S and normalizing all data by the maximum measured and computed values reveals good agreement between the measured and computed velocities, for both the source [Fig. 10(b)] and the sink [Fig. 10(d)].

Although soluto-capillary velocity profiles driven by SI source and sink beacons look quite similar (Fig. 10), DP velocity profiles do not, as noted in Sec. II B [Eqs. (43) and (44)]. Figure 11(a) shows a PEG-DA beacon sink absorbing SDS from solution, yet suspended particles exhibit no observable

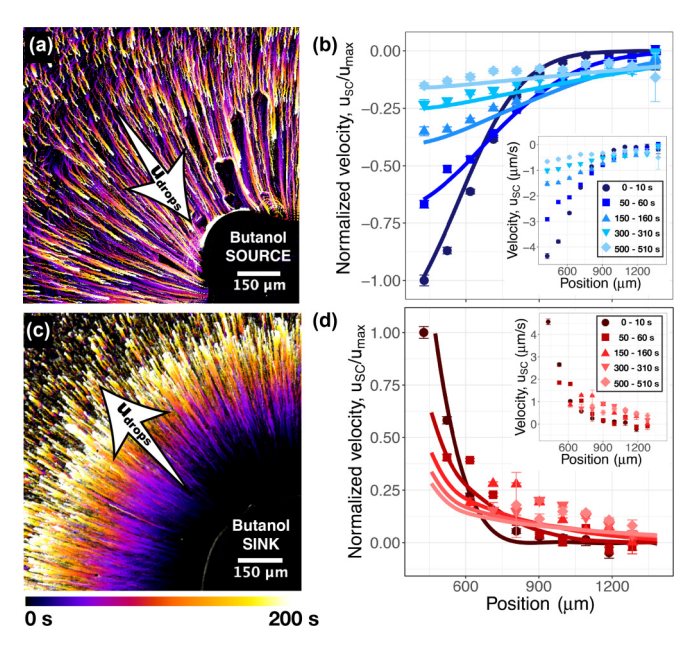


FIG. 10. Soluto-capillary migration of decane drops driven by an octanol beacon that partitions butanol. (a) A beacon source unloads butanol and attracts decane drops. (b) Migration velocities (u_{SC}) follow a ∇C_S scaling, predictions from which (lines) agree well with experimentally measured data (points). The measured and computed velocities are normalized by the maximum measured and computed values, respectively, to facilitate direct comparison between the two. Inset shows the raw experimentally tracked particle velocities. (c) Decane drops are repelled by a beacon sink that absorbs butanol from solution. (d) Points represent the measured velocities, while lines show computations based on $u_{SC} \propto \nabla C_S$ scaling. Inset shows the raw experimental data.

DP migration, in striking contrast to the long-range migration driven by source beacons that emit SDS (Fig. 9).

Figures 9–11 highlight important distinctions between drops driven by soluto-capillary migration and particles driven by DP. Soluto-capillary velocities depend on ∇C_S , whereas

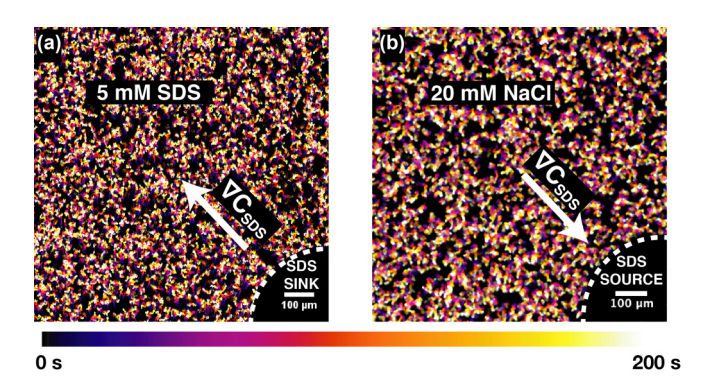


FIG. 11. Ineffective SI strategies: high background concentrations suppress DP migration. (a) A PEG-DA beacon sink absorbing SDS shows no observable SI particle migration. (b) A PEG-DA beacon source unloading SDS into a 20-mM salt solution also fails to induce colloidal motion. In both cases, the absence of any detectable particle migration is evidenced by the streak lines that show only thermal fluctuations.

DP velocities scale with $\nabla C_S/C_S$. Thus, high background solute concentrations typically give weak DP velocities, as seen for SI sinks.

In fact, high background concentrations can also suppress SI migration driven by beacon sources. For example, Fig. 11(b) shows a PEG-DA beacon source unloading SDS into a 20-mM NaCl solution. Although negatively charged polystyrene (PS) particles are expected to migrate away from SDS sources, as in Fig. 9 [5,30], the added background salt suppresses the DP migration. Therefore, while long SI times τ_{SI} are necessary for effective SI interactions over sustained durations, appreciable DP mobilities are also required.

Our experimental systems naturally introduce additional surfaces—the top and bottom of each microfluidic device potentially complicating the results beyond the difference between the 2D cylindrical SI beacon posts studied experimentally and the 3D spherical beacons studied computationally. In addition to driving suspended particles diffusiophoretically, SI solute fluxes also drive diffusio-osmotic flows along the top and bottom surfaces of the device, as reported by Ibele et al. [31], Niu et al. [10,32], and Palacci et al. [33]. In the present experiments, however, this diffusio-osmotic flow is radially symmetric and directed towards or away from the cylindrical beacon, depending on the properties of those surfaces. Simple mass conservation does not allow any depthaveraged fluid flow in the radial direction, meaning that diffusio-osmotic flows do not affect depth-averaged particle trajectories. The experiments described here were designed to be very shallow (\sim 60- μ m-tall channels) specifically to ensure that our microscopy effectively collected particles throughout the entire channel depth.

Based on the arguments presented here, we further envision freely suspended SI beacons that not only generate solute gradients but that may also migrate in response to solute fluxes, suggesting new possibilities for active matter [10,32,34–36]. For small, freely suspended beacons, however, one might expect $\tau_{\rm SI}^0$, which typically scales as R_B^2 , to be small and hence SI effects to decay quickly. To design such systems and tackle this size limitation on $\tau_{\rm SI}^0$, we predict the ideal beacon to be the one that strongly associates with solute and belongs to regime IV in the parameter map (Fig. 6). Our results suggest that solute outflux time in this regime should be limited only by the rate of solute desorption from the beacon surface and therefore be independent of the beacon size.

V. CONCLUSION

Selecting an appropriate beacon-solute combination is critical for designing soluto-inertial suspension interactions that extend over long range and that last for sustained durations. Here, we carefully examined the design space for two such beacon material choices: beacons that partition solute or that associate with solute. By mapping parameter space, we identified the limiting mass-transport processes in the distinct regimes from which we derived simple analytical expressions for the evolution of solute concentration profiles in solution. These expressions led to intuitive yet predictive approximations for the diffusiophoretic velocity profiles of particles driven by such beacons. The strategy outlined here yields a general framework that will allow users to navigate parameter

space for particular systems of interest and therefore to select appropriate materials to design these interactions.

ACKNOWLEDGMENTS

We gratefully acknowledge support from the American Chemical Society Petroleum Research Foundation (Grant No. 54141-ND5), the National Science Foundation (Grant No. CBET-1438779), and the Saudi Arabian Oil Company (Saudi Aramco, Contract No. A-0002-2018). Any opinion, findings, and conclusions or recommendations expressed in this material are those of the authors and do not necessarily reflect the views of the National Science Foundation. A portion of this work was performed in the Microfluidics Laboratory within the California NanoSystems Institute, supported by the University of California, Santa Barbara and the University of California, Office of the President, and in the Shared Experimental Facilities of the Materials Research Science and Engineering Center at UCSB (MRSEC NSF DMR 1720256).

APPENDIX: MATERIALS AND METHODS

1. COMSOL modeling

The transport of diluted species module in COMSOL MULTIPHYSICS is used to numerically solve the solute mass conservation equations. The equations are converted from a 3D coordinate system to a one-dimensional (1D) coordinate system via the following transformation:

$$\widehat{C}_i = rC_i, \tag{A1}$$

where $C_i = C_B$, C_S . The conservation equation for \widehat{C}_i ,

$$\frac{\partial C_i}{\partial t} = \frac{D_i}{r^2} \frac{\partial}{\partial r} \left(r^2 \frac{\partial C_i}{\partial r} \right),\tag{A2}$$

then becomes

$$\frac{\partial \widehat{C}_i}{\partial t} = D_i \frac{\partial^2 \widehat{C}_i}{\partial r^2}.$$
 (A3)

A similar transformation for C_{ads} and C_{free} gives

$$\frac{d\widehat{C}_{ads}}{dt} = k_1 \widehat{C}_{free} - k_{-1} \widehat{C}_{ads}, \tag{A4}$$

$$\frac{\partial \widehat{C}_{\text{free}}}{\partial t} = D_{\text{free}} \frac{\partial^2 \widehat{C}_{\text{free}}}{\partial r^2} + k_{-1} \widehat{C}_{\text{ads}} - k_1 \widehat{C}_{\text{free}}, \quad (A5)$$

where $\widehat{C}_{ads} = rC_{ads}$ and $\widehat{C}_{free} = rC_{free}$.

Transforming the variables in this manner and using the 1D solver on COMSOL enables finer mesh resolution, improving accuracy of the results, and reducing the computation time. The parametric sweep option in COMSOL is used to perform computations for several permutations and combinations of the design parameters. Results from computations are exported in matrix form and postprocessed, analyzed, and plotted on MATHEMATICA.

2. Experiments

Microfluidic devices for SI experiments are prepared as described previously [5], although partitioning beacons (octanol, Sigma Aldrich) are held in place differently than adsorbing beacons (PEG-DA). PEG-DA beacons are photopolymerized

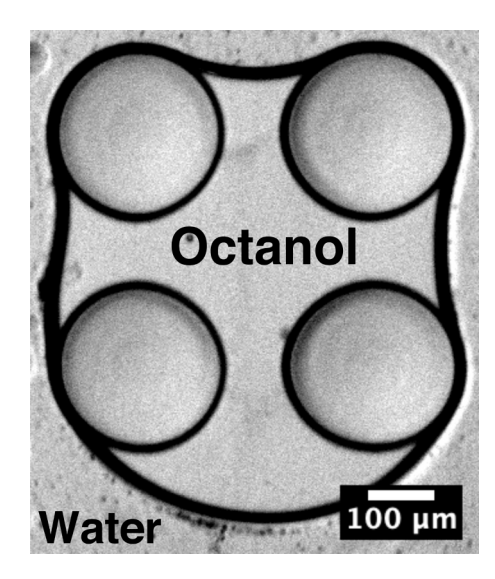


FIG. 12. Octanol beacons are held in place within a microfluidic channel by four hydrophobic gel posts surrounded by water.

in situ from precursor solution, as described in detail previously [5]. The octanol beacon, on the other hand, is trapped in the channel using four hydrophobic gel posts (Fig. 12). The posts are fabricated from a 95% vol/vol polymer (trimethylol-propane triacrylate, Polysciences) and 5% vol/vol photoinitiator (2-hydroxy-2-methylpropiophenone, Sigma Aldrich) precursor solution via the projection lithography technique used previously to fabricate the PEG-DA beacons [5]. Octanol is presaturated overnight with deionized (DI) water and then flowed into the channel. Octanol is subsequently driven out

of the channel using pressurized air, leaving an octanol drop trapped between the four hydrophobic posts. This trapped octanol then serves as the beacon.

The SI source beacons are loaded with butanol by filling channels with 0.5 M butanol (Sigma Aldrich) solution in DI water, which is left in contact with the octanol beacon for 20 min. SI experiments are initiated by introducing a suspension of surfactant-free decane drops (2% vol/vol in DI water, Sigma Aldrich). The flow is then stopped and the image series is recorded (Andor iXon 885 fluorescence camera) with a $4\times$ objective at 1 frame per second with an exposure time of 0.1 s.

SI sink experiments are performed by preparing an "empty" octanol beacon and then injecting a suspension of decane drops dispersed in 0.5 M butanol solution in DI water. The flow is then stopped, and the image series is recorded. The recorded images are subsequently imported in R programming language and analyzed via the same particle tracking routine used in our previous work [5] to obtain the particle velocity profiles.

The PEG-DA beacon in Fig. 11(a) for SI sink experiments is fabricated following the same protocol as before [5]. 5 mM SDS solution in DI water with 0.25% vol/vol negatively charged, sulfonated PS particles (1 μ m diameter, FS03F; Bangs Laboratories) is injected into the device, and then flow is stopped. Images are recorded at 1 frame per second with 0.1 s exposure time. The PEG-DA beacon source in Fig. 11(b), on the other hand, is first loaded with 5 mM SDS solution in DI water for 20 min. The SDS solution is then displaced by the PS particles dispersed in 20 mM NaCl solution, after which flow is stopped and the image series recorded.

^[1] J. N. Israelachvili, *Intermolecular and Surface Forces*, 3rd ed. (Academic Press, New York, 2011).

^[2] H. C. Hamaker, The London–van der Waals attraction between spherical particles, Physica 4, 1058 (1937).

^[3] E. M. Lifshitz, The theory of molecular attractive forces between solids, Sov. Phys. JETP 2, 73 (1956).

^[4] B. Vincent, The calculation of depletion layer thickness as a function of bulk polymer concentration, Colloids Surf. 50, 241 (1990).

^[5] A. Banerjee, I. Williams, R. N. Azevedo, M. E. Helgeson, and T. M. Squires, Soluto-inertial phenomena: Designing longrange, long-lasting, surface-specific interactions in suspensions, Proc. Natl. Acad. Sci. 113, 8612 (2016).

^[6] A. Banerjee and T. M. Squires, Long-range, selective, ondemand suspension interactions: Combining and triggering soluto-inertial beacons, Sci. Adv. 5, eaax1893 (2019).

^[7] J. J. McDermott, A. Kar, M. Daher, S. Klara, G. Wang, A. Sen, and D. Velegol, Self-generated diffusioosmotic flows from calcium carbonate micropumps, Langmuir 28, 15491 (2012).

^[8] S. Shin, O. Shardt, P. B. Warren, and H. A. Stone, Membraneless water filtration using CO₂, Nat. Commun. **8**, 15181 (2017).

^[9] D. Florea, S. Musa, J. M. R. Huyghe, and H. M. Wyss, Long-range repulsion of colloids driven by ion exchange and diffusiophoresis, Proc. Natl. Acad. Sci. USA 111, 6554 (2014).

^[10] R. Niu, D. Botin, J. Weber, A. Reinmüller, and T. Palberg, Assembly and speed in ion-exchange-based modular phoretic microswimmers, Langmuir 33, 3450 (2017).

^[11] R. Guha, F. Mohajerani, A. Mukhopadhyay, M. D. Collins, A. Sen, and D. Velegol, Modulation of spatiotemporal particle patterning in evaporating droplets: Applications to diagnostics and materials science, ACS Appl. Mater. Interfaces 9, 43352 (2017).

^[12] D. Velegol, A. Garg, R. Guha, A. Kar, and M. Kumar, Origins of concentration gradients for diffusiophoresis, Soft Matter 12, 4686 (2016).

^[13] B. V. Derjaguin, S. S. Dukhin, and A. A. Korotkova, Diffusiophoresis in electrolyte solutions and its role in the mechanism of the formation of films from caoutchouc latexes by the ionic deposition method, Prog. Surf. Sci. 43, 153 (1993).

^[14] D. C. Prieve, Migration of a colloidal particle in a gradient of electrolyte concentration, Adv. Colloid Interface Sci. 16, 321 (1982).

^[15] D. C. Prieve, J. L. Anderson, J. P. Ebel, and M. E. Lowell, Motion of a particle generated by chemical gradients, Part 2. Electrolytes, J. Fluid Mech. 148, 247 (1984).

^[16] J. L. Anderson, Colloid transport by interfacial forces, Ann. Rev. Fluid Mech. 21, 61 (1989).

- [17] V. G. Levich and A. M. Kuznetsov, Motion of drops in liquids under the influence of surface-active substances, Dokl. Akad. Nauk SSSR 146, 145 (1962).
- [18] A. Leo, C. Hansch, D. Elkins, Partition coefficients and their uses, Chem. Rev. 71, 525 (1971).
- [19] American Pharmaceutical Association and Academy of Pharmaceutical Sciences, Partition Coefficient: Determination and Estimation, edited by W. J. Dunn, J. H. Block, and R. S. Pearlman (Pergamon Press, New York, 1986) Available from: https://books.google.com/books?id=uxBtAAAAMAAJ.
- [20] J. Sangster, Octanol-water partition coefficients of simple organic compounds, J. Phys. Chem. Ref. Data 18, 1111 (1989).
- [21] E. Yariv and I. Frankel, The Diffusion-Control Limit Revisited, Phys. Rev. Lett. 89, 266107 (2002).
- [22] J. L. Anderson, M. E. Lowell, and D. C. Prieve, Motion of a particle generated by chemical gradients, Part 1. Non-electrolytes, J. Fluid Mech. 117, 107 (1982).
- [23] E. M. Ahmed, Hydrogel: Preparation, characterization, and applications: A review, J. Adv. Res. 6, 105 (2015).
- [24] D. Zhao, J. Feng, Q. Huo, N. Melosh, G. H. Fredrickson, B. F. Chmelka, and G. D. Stucky, Triblock copolymer syntheses of mesoporous silica with periodic 50 to 300 angstrom pores, Science 279, 548 (1998).
- [25] S. Wintzheimer, T. Granath, M. Oppmann, T. Kister, T. Thai, T. Kraus, N. Vogel, and K. Mandel, Supraparticles: Functionality from uniform structural motifs, ACS Nano. 12, 5093 (2018).
- [26] B. Amsden, Solute diffusion within hydrogels, Mechanisms and models, Macromolecules **31**, 8382 (1998).
- [27] B. Amsden, Solute diffusion in hydrogels: An examination of the retardation effect, Polym. Gels Networks 6, 13 (1998).

- [28] E. L. Cussler, *Diffusion: Mass Transfer in Fluid Systems*, 3rd ed., Cambridge Series in Chemical Engineering (Cambridge University Press, Cambridge, England, 2009).
- [29] J. Kim, Y. Gao, C. Hebebrand, E. Peirtsegaele, and M. E. Helgeson, Polymer-surfactant complexation as a generic route to responsive viscoelastic nanoemulsions, Soft Matter 9, 6897 (2013).
- [30] R. Nery-Azevedo, A. Banerjee, and T. M. Squires, Diffusiophoresis in ionic surfactant gradients, Langmuir 33, 9694 (2017).
- [31] M. Ibele, T. Mallouk, and A. Sen, Schooling behavior of light-powered autonomous micromotors in water, Angew. Chem., Int. Ed. 48, 3308 (2009).
- [32] R. Niu, T. Palberg, and T. Speck, Self-Assembly of Colloidal Molecules Due to Self-Generated Flow, Phys. Rev. Lett. 119, 028001 (2017).
- [33] J. Palacci, S. Sacanna, A. P. Steinberg, D. J. Pine, and P. M. Chaikin, Living crystals of light-activated colloidal surfers, Science 339, 936 (2013).
- [34] I. Theurkauff, C. Cottin-Bizonne, J. Palacci, C. Ybert, and L. Bocquet, Dynamic Clustering in Active Colloidal Suspensions with Chemical Signaling, Phys. Rev. Lett. 108, 268303 (2012).
- [35] P. G. Moerman, H. W. Moyses, E. B. van der Wee, D. G. Grier, A. van Blaaderen, W. K. Kegel, J. Groenewold, and J. Brujic, Solute-mediated interactions between active droplets, Phys. Rev. E 96, 032607 (2017).
- [36] B. Liebchen, R. Niu, T. Palberg, and H. Löwen, Unraveling modular microswimmers: From self-assembly to ion-exchangedriven motors, Phys. Rev. E 98, 052610 (2018).